Biophysical Journal Volume 96 January 2009 67–76

Sphingomyelinase-Induced Domain Shape Relaxation Driven by Out-of-Equilibrium Changes of Composition

Maria Laura Fanani,[†*] Luisina De Tullio,[†] Steffen Hartel,[‡] Jorge Jara,[§¶] and Bruno Maggio[†]
[†]Departamento de Química Biológica, Centro de Investigaciones en Química Biológica de Córdoba, Facultad de Ciencias Químicas, Universidad Nacional de Córdoba, Argentina, Haya de la Torre y Medina Allende, Ciudad Universitaria, Córdoba, Argentina; [‡]Anatomy and Development Biology Program, Faculty of Medicine, Universidad de Chile; [§]School of Civil Engineering in Computer Science, Universidad Austral de Chile, Valdivia, Chile; and [¶]Centro de Estudios Científicos, Valdivia, Chile

ABSTRACT Sphingomyelinase (SMase)-induced ceramide (Cer)-enriched domains in a lipid monolayer are shown to result from an out-of-equilibrium situation. This is induced by a change of composition caused by the enzymatic production of Cer in a sphingomyelin (SM) monolayer that leads to a fast SM/Cer demixing into a liquid-condensed (LC), Cer-enriched and a liquid-expanded, SM-enriched phases. The morphological evolution and kinetic dependence of Cer-enriched domains is studied under continuous observation by epifluorescence microscopy. Domain shape annealing is observed from branched to rounded shapes after SMase activity quenching by EDTA, with a decay halftime of ~10 min. An out-of-equilibrium fast domain growth is not the determinant factor for domain morphology. Domain shape rearrangement in nearly equilibrium conditions result from the counteraction of intradomain dipolar repulsion and line tension, according to McConnell's shape transition theory. Phase separation causes a transient compositional overshoot within the LC phase that implies an increased out-of-equilibrium enrichment of Cer into the LC domains. As a consequence, higher intradomain repulsion leads to transient branched structures that relax to rounded shapes by lowering the proportion of Cer in the domain to equilibrium values. The fast action of SMase can be taken as a compositional perturbation that brings about important consequences for the surface organization.

INTRODUCTION

Over the years, evidence has accumulated indicating that the lipid distribution in biomembranes is nonrandom (1). In relation to membrane-associated enzyme activities, lipid mixing-demixing processes and the concomitant structuring of segregated domains with different lipid composition or phase state profoundly influences precatalytic and catalytic steps of phosphohydrolytic reactions (2–6). A group of phospholipases called Sphingomyelinases (SMases) hydrolyze the membrane constituent sphingomyelin (SM) to phosphocholine and ceramide (N-acylsphingosine) (Cer), a second messenger involved in cell signaling (7). Fundamental cellular processes such as proliferation, differentiation, and cell death are triggered by the temporal local production of Cer by different SMases (8,9). Cer was reported to induce the formation of laterally segregated gel (bilayers) or liquid-condensed (LC)(monolayers) domains in several systems (5,10–12). Different morphologies of Cer-enriched domains, as reported from monolayer experiments, depend on both the type and the proportion of Cer in lipid mixtures with SM (5) or with dimyristoylphosphatidylcholine (13). Also, formation of segregated domains enriched in Cer has been involved in membrane protein segregation and cellular function (14,15).

In previous work we provided the first, to our knowledge, direct visual evidence in real-time for SMase-induced formation of Cer-enriched domains in SM monolayers under precise control of the surface intermolecular packing (5). A bidirectional communication between effects taking place at the local catalytic level and the supramolecular surface organization were described. Further studies disclosed a series of morphologic domain transitions and formation of defined hexagonal surface lattices of the evolving SMase-generated Cer-enriched domains at particular times of the phosphohydrolytic reaction. A close analysis of these effects revealed the significance of underlying physical properties such as line tension and dipolar electrostatic repulsion (16) in controlling the shape of the domains and their long range organization.

Changes of the initial topography and lipid composition modulate the degradation of SM by SMase. The amount of lateral interface is a parameter that appears to determine the attainment of precatalytic steps necessary for reaching full activity (17). A novel mechanism was proposed recently for the action of SMase that can also explain the regulatory effect of the surface topography on enzyme activity (6). SMase acts through an area-activated mechanism, whereby Cer is produced homogeneously in the liquid expanded (LE) SM-enriched phase, leading to Cer supersaturation. At this point product-induced inhibition of SMase by Cer (18) occurs in the homogeneous LE phase. Cer supersaturation, beyond a critical limit, acts as a driving force for nucleation of a Cer-enriched segregated LC phase according to classical nucleation theory. SM/Cer demixing leads to a SM-enriched LE phase with a relatively low proportion of Cer that allows the enzymatic activity to proceed in steady-state rate according to enzyme localization. The

Submitted July 3, 2008, and accepted for publication August 27, 2008.
*Correspondence: lfanani@gmail.com
Editor: Lukas K. Tamm.

0006-3495/09/01/0067/10 $2.00
doi: 10.1529/biophysj.108.141499

kinetic barrier for domain nucleation can partially explain the lag time of the reaction before achieving the steady-state catalytic condition (6).

In most studies related to enzyme action and regulation, equilibrium conditions are assumed, whereas active and functional membranes are far from equilibrium structures, or in a steady state controlled by fluxes of energy and matter. Thus, thermodynamic nonequilibrium effects should have direct relevance to the lateral organization of membrane components. Several studies documented differences between the enzymatic production and the direct Cer incorporation to both bilayer and monolayer lipid system (5,10,11,19,20). Previous work from our group (5) showed that a relatively rapid (<15 min) enzymatic generation of Cer by SMase in SM monolayers leads to a different surface topography than that acquired by enzyme-free premixed SM/Cer monolayers of the same lipid composition. As a consequence, selective structural information is stored depending on the manner in which the surface was generated. Detailed topographical features of both types of monolayers are substantially different as follows (5,16): 1), domains formed by the action of SMase show regular sized star-like shape whereas condensed rounded domains are observed in the enzyme-free films; 2), in the SMase treated monolayer the interdomain structuring appears to self-organize into highly ordered hexagonal lattice patterns, whereas less ordered structures are seen in enzyme-free SM/Cer monolayers; and 3), only in the case of the enzyme-free SM/Cer monolayers, do the LC domains formed cover an area whose relatively large size can not be accounted for by a phase of pure Cer. These findings can be interpreted as a consequence of an out-of-equilibrium state of the SMase-driven SM→Cer conversion. Evidences on these phenomena have been pointed out by other authors. In lipid bilayers (vesicles and supported bilayers) it was reported that the rapid conversion of SM to Cer by SMase drives the membrane domain structure into a metastable state, subsequently relaxing to a new organization (10,20). As described herein, the existence of an out-of-equilibrium condition of the lipid monolayer after a fast enzymatic Cer production can be experimentally tested.

The kinetics of lipid demixing (phase separation) has been addressed previously for simple phospholipid mixtures (21,22) both from the experimental and theoretical point of view. In those cases the nonequilibrium situation was induced by a sudden thermal quench from a one-fluid phase equilibrium situation (high temperature) to the gel/fluid coexistence range (low temperature). The attainment of equilibrium in this conditions is a very slow process (occurring over a timescale of hours), leading to large domains at infinite time. In this work the nonequilibrium situation is induced by a change of composition caused by the action of SMase. We studied the kinetics of phase demixing of SM/Cer monolayers under continuous observation by epifluorescence microscopy. A transient compositional overshoot within the domains enriched in Cer is evidenced in the case of fast enzymatic reaction that brings about important consequences for the subsequent changes of domain shape and surface organization.

EXPERIMENTAL PROCEDURES

Chemicals

Bovine brain SM bovine brain Cer and *Bacillus cereus* sphingomyelinase (SMase) (EC 3.1.4.12) were purchased from Sigma-Aldrich (St. Louis, MO). The lipids were over 99% pure by thin layer chromatography and were used without further purification. The lipophylic fluorescent probe 1,1′-didodecyl-3,3,3′3′-tetramethylindocarbocyanine perchlorate ($DiIC_{12}$) was purchased from Molecular Probes (Eugene, OR). Solvents and chemicals were of the highest commercial purity available. The water was purified by a Milli-Q-system, to yield a product with a resistivity of ~18.5 MΩ/cm. Absence of surface active impurities was routinely checked as described elsewhere (23).

Epifluorescence microscopy of lipid monolayers

Monolayers of pure SM doped with 1 mol % $DiIC_{12}$, a probe that preferably partitions into liquid-expanded phase, were spread from lipid solutions in chloroform/methanol (2:1) over a subphase of 10 mM Tris/HCl, 125 mM NaCl, 3mM MgCl, pH 8, until reaching a pressure of less than ~0.5 mN/m (24). After solvent evaporation (10 min), the monolayer was slowly compressed to the desired surface pressure (π = 10 mN/m). The monolayer equipment (Kibron μ-Trough S; Kibron, Helsinki, Finland) was mounted on the microscope stage. Epifluorescence visualization was carried out on a Zeiss Axioplan microscopy (Carl Zeiss, Oberkochen, Germany) using a mercury lamp (HBO 50), and a 20X LD objective. Images with exposure times of ~60ms were taken continuously (snapshoot every 3s) with a CCDcamera (Micromax, Princeton Instruments, Downingtown, PA) controlled by Metamorph 3.0 (Universal Imaging, Union City, CA) software. All the experiments were carried out in an air conditioned room (22 ± 2°C).

Determination of SMase activity

For SMase-induced domain imaging the enzyme was injected into the subphase of the circular reaction compartment (3 mL; 3.14 cm^2) of an all-Teflon zero-order trough under stirring, as described before (24). After the injection of SMase (0.5–6 mU/mL) SM is converted to phosphocholine and Cer. Phosphocholine solubilizes into the subphase, whereas Cer remains at the interface. The reaction compartment is monitored by epifluorescence microscopy and Cer-enriched domain formation and growth is registered continuously by time series images. Due to the difference in cross-sectional area between SM and Cer (84 $Å^2$ and 51 $Å^2$ at 10mN/m respectively) the reaction progress can be followed in real time by the reduction of the total monolayer area. A reservoir compartment adjacent to the reaction compartment and connected by a narrow and shallow slit serves as substrate monolayer reservoir (pure SM) and allows the measurement of surface pressure. As the reaction takes place, the total monolayer area is automatically adjusted to keep the surface pressure constant (at 10 mN/m) through the movement of a barrier in the reservoir compartment. This allows for keeping the reaction compartment area constant during the reaction course even though the total area decreases (5,16).

SMase-generated domain shape relaxation

For domain shape relaxation experiments, the reaction was assayed in the absence of the cofactor Mg^{2+} to reach a more efficient and rapid catalytic quench by EDTA. In this condition, 10 times more enzyme than in the presence of Mg^{2+} (5–60 mU/mL) were necessary to reach similar catalytic activity (0.1–3.0 × 10^{13} molecules·min^{-1}·cm^{-2} under steady-state catalysis). When the reaction

reaches a period corresponding to about half the time of pseudo zero-order kinetics (18,25), SMase action was quenched by an injection of EDTA into the subphase of the reaction compartment (final concentration 170 mM) followed by a 1 min stirring. SMase quenching is established when no movement of the mobile barrier is necessary to keep the surface pressure constant. After we checked that the catalytic activity had fully stopped within an error of ±5 mol% (10 min after EDTA injection), the reaction compartment was disconnected from the reservoir compartment. Since the reservoir monolayer is composed of pure SM, release of Cer molecules produced in the reaction compartment to the reservoir does occur before the compartment disconnection (<10% of domains are lost). For this reason, analysis of total liquid-condensed area (the sum of domains area) or number of domains in relaxation experiments is not reliable and this work focuses solely on the domain shape analysis. Domain shape relaxation was followed by imaging every 3–5s for up to 3 h.

Computational analysis of surface topography

For each experiment, 25–35 images were used for domain shape characterization. LE and LC lipid phases are represented by bright (high fluorescence/$DiIC_{12}$-enriched) and dark (low fluorescence/$DiIC_{12}$-depleted) pixels respectively in the 8-bit intensity interval of the fluorescent images ($I \in [0,255]$, 225.5 × 175 μm, 886 × 692 pixel) (Fig. 1 *A*). A gross segmentation of $DiIC_{12}$-depleted domains was achieved by interactive image processing routines written in Interactive Data Language (ITT, Boulder, CO) which only provides a gross estimation of the domain border (Fig. 1 *B*) (16). The segmentation of Cer-enriched domain borders was optimized by the following steps: 1), as outlined in (17), the separation of bright and dark regions into binary object masks for the Cer- and SM-enriched domains was achieved by a combination of boundary detection filters, followed by a successive treatment of pixel erosion and dilatation operations. For experimental settings where the lipid domain size and the undulations of its boundaries are large in comparison to the pixel size, the applied segmentation introduces an artificially high number of border saddle points which does not represent the undulations observed in the original image (white crosses mark saddle points of the parametric curves in Fig. 1 *C*). 2), we solved this problem using an active contour model, a parametric curve $\underline{C}(s) = [x(s), y(s)]$, $s \in [0, 1]$, is initiated with the border trajectory of the first segmentation (26). The contour points $[x_i, y_i]$ are subjected to internal forces like elasticity (α) or rigidity (β), which mimic line tension or curvature representing physical properties of a deformable contour. 3), These internal forces of the parametric curve $\underline{C}(s)$ interact with external force fields that are derived from the intensity gradients and Laplacians of the original image matrix I[x,y] by an iterative algorithm based on Generalized Gradient Vector Flows (27). Finally, 4), balance between internal and external forces is computed iteratively by the Euler-Lagrange condition for the minimization of the energy functional E for the parametric curve $\underline{C}(s)$:

$$E = \int_0^1 0.5 \times \left[\alpha\left|\underline{C}'(s)\right|^2 + \beta\left|\underline{C}''(s)\right|^2\right] + E_{\text{ext}}(\underline{C}(s))ds, \quad (1)$$

$\underline{C}'$ and $\underline{C}''$ denominate first and second order derivatives with respect to s. Precise assimilation of the contours toward the morphology of the Cer-enriched domains was achieved by setting the appropriate combination of model parameters (Fig. 1 *D–E*).

In addition to α and β, the model parameters include viscosity (γ), external force (k), minimum distance between adjacent contour points (f), and number of iterations (t) (26,27). The optimized domain contour $\underline{C}(s)$ forms the basis for the quantitative description of the domain morphologies. The number of domain branches was calculated as half the number of inflection points of $\underline{C}(s)$. A circular or oval domain has no inflection point, although each branch (concavity or convexity) is characterized by two inflection points. In addition, we calculated the zoom-invariant descriptor of circularity perimeter^2/area (P^2/A), for domains with perimeter (P) and area (A). For perfect circles, P^2/A yields 4π, whereas any shape deviation from a circle leads to $P^2/A > 4\pi$.

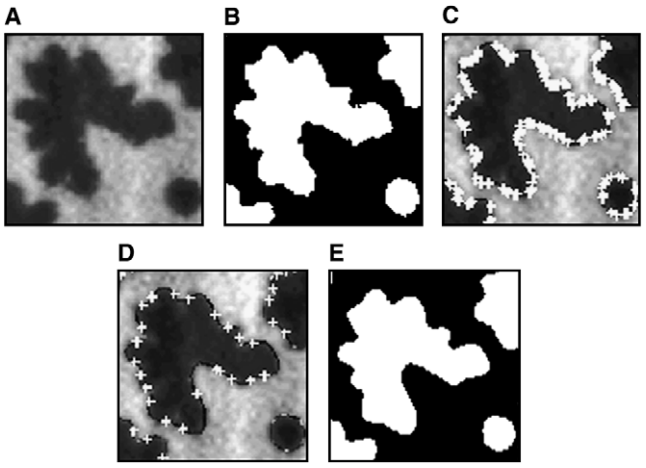

FIGURE 1 Segmentation of Cer-enriched domain borders with active contours. (*A*) Epifluorescence image with two representative Cer-enriched domains. (*B*) A threshold based segmentation of Cer-enriched domains only provides a gross estimation of the domain border. (*C*) A first approximation of Cer-enriched domain borders by active contours C(s) is initialized by the segmented object boundaries (*B*). For all cases white crosses mark saddle points of the parametric curves. (*D*) Active contours C(s) after 10 iterations reveal the number of border undulations of Cer-enriched domains in a reliable manner. (*E*) Final segmentation of Cer-enriched domains for the subsequent calculation of morphologic features (for details see Experimental Procedures section).

RESULTS AND DISCUSSION

In previous work we demonstrated that SMase driven SM → Cer conversion in pure SM monolayers takes place homogeneously within the LE phase, where the enzyme is located (6). The supersaturation of Cer in this phase leads, beyond a critical limit, to nucleation of laterally segregated, Cer-enriched (LC) domains. This phenomenon was found to fit classical nucleation theory, with the number of nuclei formed being proportional to the degree of supersaturation of Cer in the LE phase (acting as a driving force). After the nucleation event, domains grow by addition of Cer molecules newly produced within the LE phase (6) producing Cer-enriched domains that exhibit regularly undulated (flower-like) shapes (5,16).

We previously reported (5) that the relatively rapid (in <15 min) enzymatic generation of Cer by SMase activity on SM monolayers leads to Cer-enriched domains with important morphological differences than Cer-enriched domains observed in enzyme-free SM/Cer mixed monolayers of the same composition. Domains formed by the action of SMase show regular sized star-like shape whereas condensed round domains are observed in the enzyme-free films (5,16). These phenomena can be interpreted as a consequence of SMase activity driving the system to an out-of-equilibrium state. Studies by other authors with supported bilayers treated with SMase similarly suggested that slow evolution

of the domain topography occurred over a period of 1 h or more after the enzyme activity was presumably halted; unfortunately, the methods used did not allow for ascertaining defined details of domain morphology and its relaxation features (20). Earlier studies in bilayer vesicles proposed that, although the hydrolytic reaction could be rapidly completed (i.e., within <3 min), the reorganization of Cer into domains required times of 100 min or more, evidencing a dependence of the Cer production rate on the bilayer organization (10).

To further the conception of the morphology and surface organization of the SMase-induced Cer-enriched domains as structures resulting from an out-of-equilibrium process, we studied the morphologic evolution and dependence on enzyme kinetic of the SMase-induced Cer-enriched LC domains immersed in a continuous fluid phase.

Shape complexity was analyzed by determining the number of branches of the Cer-enriched domains and the area-invariant descriptor of circularity P^2/A. White crosses in Fig. 1 show inflection points on the domain border trajectory; two inflection points account as a branch on domain shape. P^2/A yields 12.5 (4π) for a perfect circle and yields higher values for shapes deviating from circularity. The reliable quantification of morphologic domain parameters was guaranteed by the application of the active contour model (see Experimental Procedures section and Fig. 1).

Experiments were performed where the activity of SMase during the steady-state reaction and before the time of percolation of the LC domains was halted by EDTA injection in the subphase (Fig. 2 *A*). After stopping Cer production (within ± 5 mol %), the domain morphology is monitored by a period of 1–3h. Fig. 2 shows the time evolution of a representative monolayer after SMase halting. Annealing to rounded shapes is observed in Fig. 2, *B–D* and is clearly reported by the shape descriptors (Fig. 2, *E–F*); these parameters reach near-equilibrium values ~80–100 min after EDTA injection. Domain shape annealing can be described as a single exponential decay process (Fig. 2, *E–F*) with a relaxation half time of ~11–13 min.

To explore if the relaxation process depends on the initial shape of the domains and equilibrium conditions where these domains were grown, we analyzed the annealing of SMase-induced domains generated under different rates of production of Cer by SMase. Fig. 3 shows a biphasic behavior of domain complexity with the increase of Cer production rate (Fig. 3, *left panel*) with a peak in domain branching observed in Fig. 3 *B left panel*. For the slowest experiment almost no domain border undulations are formed during the reaction time (Fig. 3 *A*). In this case, the reaction is closer to equilibrium than in any other condition used and rounded shapes dominate. Fig. 3 (*right panel*) shows images of the

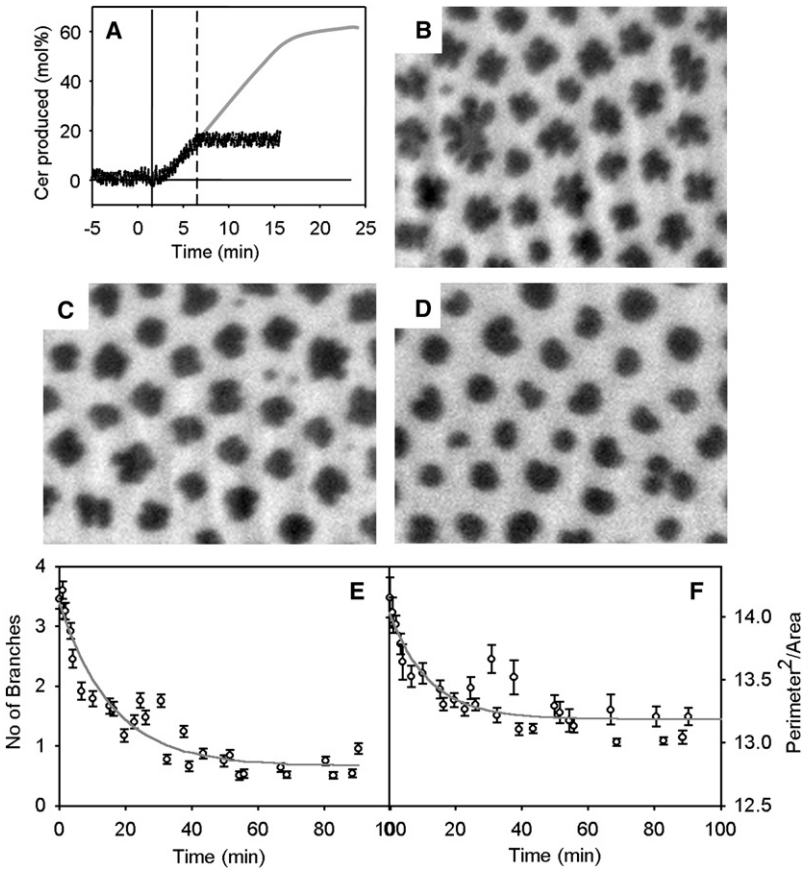

FIGURE 2 Domain shape relaxation after SMase halting. (*A*) Time course of the SMase-catalyzed SM→Cer conversion. The full vertical line shows the time of SMase injection into the subphase (final concentration 42 mU/mL, two-dimentional enzymatic rate 2.5 ± 0.1 × 10^{13} molec·min^{-1}·cm^{-2}) and dashed line shows the time of SMase halting by EDTA injection into the subphase (final concentration 170 mM). The reaction was carried out in the absence of the cofactor Mg^{2+} to optimize the activity stopping. The gray lines illustrate the time course of a similar experiment not treated with EDTA. (*B–D*) Epifluorescence representative images of the $DiIC_{12}$-labeled monolayer at 4, 20 and 100 min after SMase halting. Image size is 112 × 87 μm. (*E–F*) Time dependence of domain shape parameters: number of branches and perimeter^2/area after SMase halting. The values correspond to averages of 100–130 domains ±SE. The gray line represents the fitted curve of the experimental data with a single exponential decay equation. All the data shown corresponds to the same representative experiment.

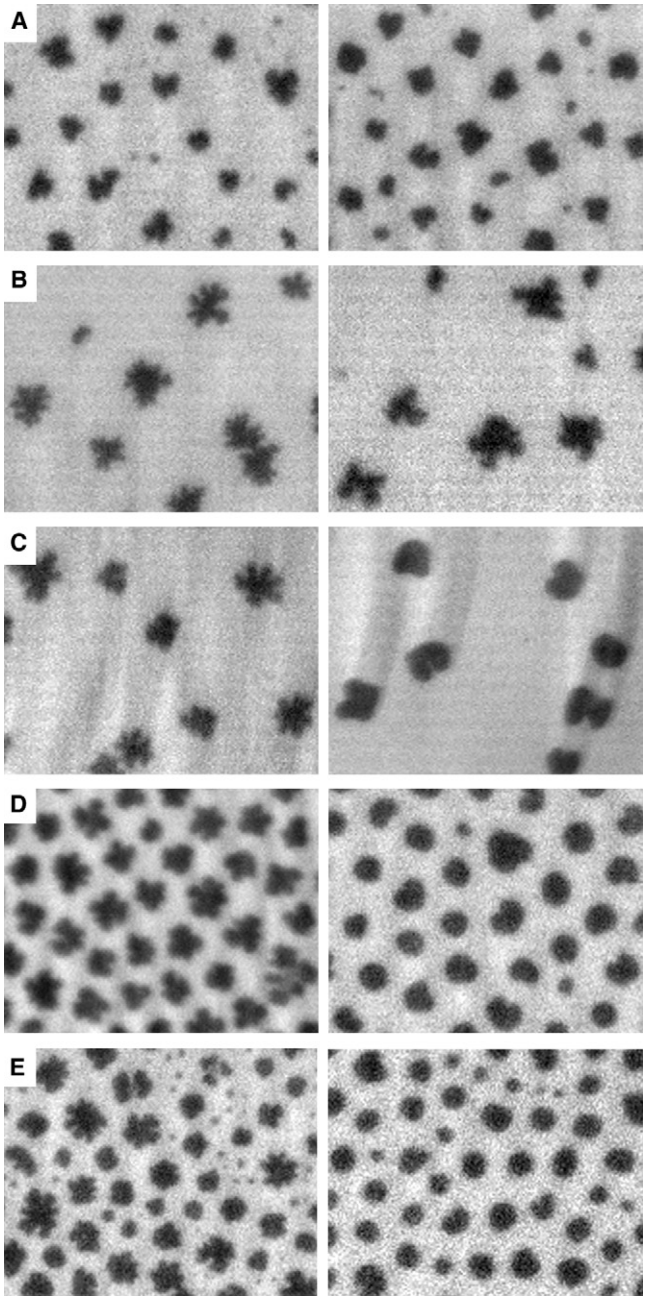

FIGURE 3 Representative images showing domain shape relaxation under different Cer-production rates by SMase. The epifluorescence micrographs illustrate $DiIC_{12}$-labeled SM monolayers under SMase action, immediately after SMase halting (*left panels*) or after domain relaxation (shape parameters remain constant with time within 5%), (*right panel*). The five single experiments (*A–E*) were performed under conditions of increasing Cer-production rates. Final subphase SMase concentrations are from *A* to *E*: 2, 13, 34, 42 and 45 mU/mL respectively giving a two-dimensional enzymatic rate of: $0.13 \pm 0.02, 0.80 \pm 0.05, 2.0 \pm 0.1, 2.5 \pm 0.1$ and $3.1 \pm 0.6 \times 10^{13}$ (molec$\cdot$min$^{-1}\cdot$cm^{-2}). Image size is 112×87 μm. For reaction conditions details see legend of Fig. 2 and Experimental Procedures section.

same experiments after shape annealing. The time at which this stage is reached ranges from 30 to 180 min (with shape parameters values remaining constant within $\pm 5\%$) depending on the initial conditions (Fig. 4, *A–B*). The decay process for experiments (Fig. 3, *A–E*) is analyzed in Fig. 4, *A–B* (*curves a–e*). For the sake of simplicity only the fitted curves are shown. The half time of those relaxation processes appears not to significantly depend on the initial condition (size and shape of domains) (Fig. 4 *C*), supporting a robust kinetics of the relaxation mechanism. Fig. 4, *D–E* shows that the shape parameters analyzed as a function of the Cer production rate show a bell shape variation both before and after shape annealing, with a maximum close to a rate of 0.75×10^{13} (molec$\cdot$min$^{-1}\cdot$cm^{-2}). A maximum shape relaxation is observed above this rate. It is worth emphasizing that the equilibrium shape adopted in each case does strongly depend on the initial domain conditions (Fig. 3, *right panels*, and Fig. 4, *D–E*). The significance of this observation is analyzed below.

A question arising from these results is what might be the physical forces/mechanism that lead to the out-of-equilibrium border undulated shapes of Cer-enriched domains? Two experimentally testable mechanisms are considered to attempt a deeper understanding of this phenomenon: 1), domain shape is an out-of-equilibrium process as a consequence of fast domain growth; and 2), the composition of the two coexisting phases is out-of-equilibrium as a consequence of a slow SM/Cer demixing process.

As Miller et al. (28) first reported for dimyristoyl-phosphatidyl-ethanolamine monolayers under conditions exhibiting the LE-LC phase transition, dendritic-shaped domains are formed after a fast compression above the transition pressure. These structures showed self-similarity with a fractal dimension $d = 1.5 \pm 0.1$, and were related to the process described by the theoretical diffusion-limited aggregation (DLA) model (29). This model considers that the random aggregation of monomers to a crystalline structure, when the growing kinetics depends only on the monomer diffusion rate and no activation energy is necessary for the aggregation step, should give a fractal (dendritic like) structure with a dimension about $d = 1.67$. Miller's domains showed structural annealing to more rounded shapes attributed to slow changes caused by the action of the line tension (with a kinetics of minutes). Theoretical analysis (Monte Carlo simulation) of a two-dimension model that undergoes a thermally driven fluid-solid phase transition controlled by vacancy diffusion (30) exhibits the formation of fractal domain growth at early times and crossover to compact solidification as equilibrium is approached.

Taking into account that SMase-induced domains were previously reported to show self-similarity, with a fractal dimension in the range of 1.63–1.76 (16) and the results reported in our work, SMase-generated Cer-enriched domains can fit the behavior described for Miller's domains (21). Therefore, the regular undulation of the LC-domain borders during rapid domain growth in an out-of-equilibrium conditions might be a consequence of aggregation mechanisms (DLA like) resulting from Cer being produced within the SM-enriched LE phase (6).

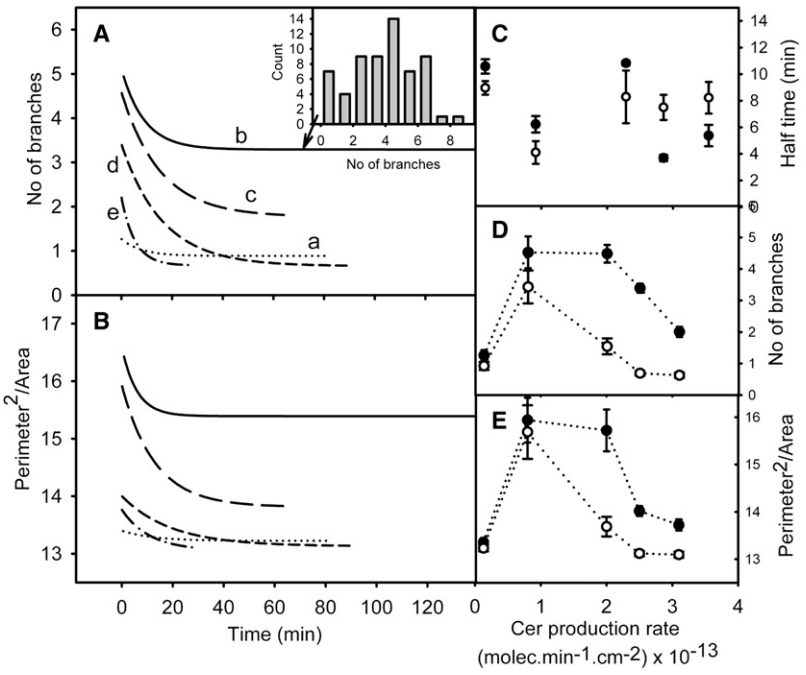

FIGURE 4 Domain shape relaxation under different Cer-production rates. (*A–B*) Time dependence of domain shape parameters (number of branches and perimeter^2/area) after SMase halting for five experiments proceeding at different Cer production rates (two-dimensional enzymatic activity 0.13 ± 0.02, 0.80 ± 0.05, 2.0 ± 0.1, 2.5 ± 0.1 and 3.1 ± 0.6 × 10^{13} molec·min^{-1}·cm^{-2} for experiments *a-e* respectively). Experiments *a–e* corresponds to experiments *A–E* in Fig. 3. The inset represents the histogram distribution of the number of branches for four pictures (N^o domains analyzed = 61) of experiment *b* after shape relaxation. Experiment *b* was allowed to relax for more than 3hs with no further change in domain shape. For simplicity only the fitted curves (exponential decays) are shown. (*C*) Decay half times for the curves shown in Fig. 4, *A–B*. Solid circles represent the experimental value for the number of branches decay, open circles are for perimeter^2/area decay. Error bars represent SE. (*D–E*) Comparison between the domain shape parameters from four pictures took 2–4 min after SMase halting (*solid circles*) and after shape relaxation (*open circles*) for experiments *a–e*. The ''after shape relaxation'' time for each experiment is the time after which shape parameters values keep constant (within ±5%) and it depends on each case. Error bars are ±SE and lines are drawn as a tendency to guide the eye and are not intended to represent a continuous correlation.

To test this hypothesis we studied the complexity of domains generated at different Cer production rates while keeping similar domain size and domain growth rates. Fig. 5 shows that domains formed at a fast Cer production rate (equivalent to the fastest experiment seen in Fig. 4) exhibit highly undulated border morphology (Fig. 5 *A*) whereas domains formed at a low Cer production rate (20 folds lower, equivalent to the slower experiment seen in Fig. 4) exhibit poorly undulated borders (Fig. 5 *B*) even though the domain growth rate in both cases is similar (Fig. 5 *C*). The morphological differences at comparable domain size (~80 μm^2) are highlighted by the shape parameter ''number of branches'' in Fig. 5 *D*.

The DLA mechanism implies that the rate of domain growth determines its morphology in such a way that a fast growth should correspond to increasingly fractal (higher number of branches) structures. Therefore, domains growing at similar rates and of comparable size should present similar shape. Fig. 5 shows the shape analysis of domains formed under high and low Cer production rates where the domain growth rate is similar. This is possible since the overall LC phase growth is higher for the faster SMase-catalyzed reaction but, concomitantly, the number of domains is also larger (Fig. 5 *A–B*). Domains in both conditions show different domain structures. This leads to the conclusion that an out-of-equilibrium fast domain growth can not be the sole determinant factor for domain morphology. Further support for this conclusion is the finding that for any experimental condition explored there is always a domain size (critical area, A_c) for which domains under this limit exhibit nearly rounded shapes (Fig. 5 *A*, *white arrow*). If a fast growing rate was determinant for the appearance of border-undulated domain morphology, this fractal-like structure should be present at any domain size, as far as the image is above the resolution limit. Therefore, the domain morphology rearrangement appears to be fast enough to be kept in nearly equilibrium conditions along the domain growth curve.

The annealing of Cer-enriched domains produced by the fast action of SMase may be interpreted as a consequence of a slow and complex SM/Cer demixing process that induces a slow local compositional change of the LC phase (domains). This effect leads to changes in the equilibrium shape of the domains in terms of the Mohwald/McConnell shape transition model (31,32).

McConnell's shape transition theory under equilibrium conditions implies that domain shape is a consequence of two counteracting forces: the line tension at the domain boundary (λ) and the difference in the resultant perpendicular dipole moment density (μ) between the molecules in the coexisting phases. A high value of λ tends to minimize the domain border favoring rounded shapes, whereas high values of μ involve internal intermolecular repulsion that should result in domain elongation or branching. These two forces equilibrate each other at the critical domain size A_c where the transition between round to border-undulated shapes occurs. At this critical point R_c, the average radius of the circular domain of size A_c can be described as follows:

$$R_c = \frac{d}{4} e^{Zm} e^{(\lambda/\mu^2)}, \qquad (2)$$

where d is the separation distance between neighboring dipoles and Zm is the shape transition exponent defined by

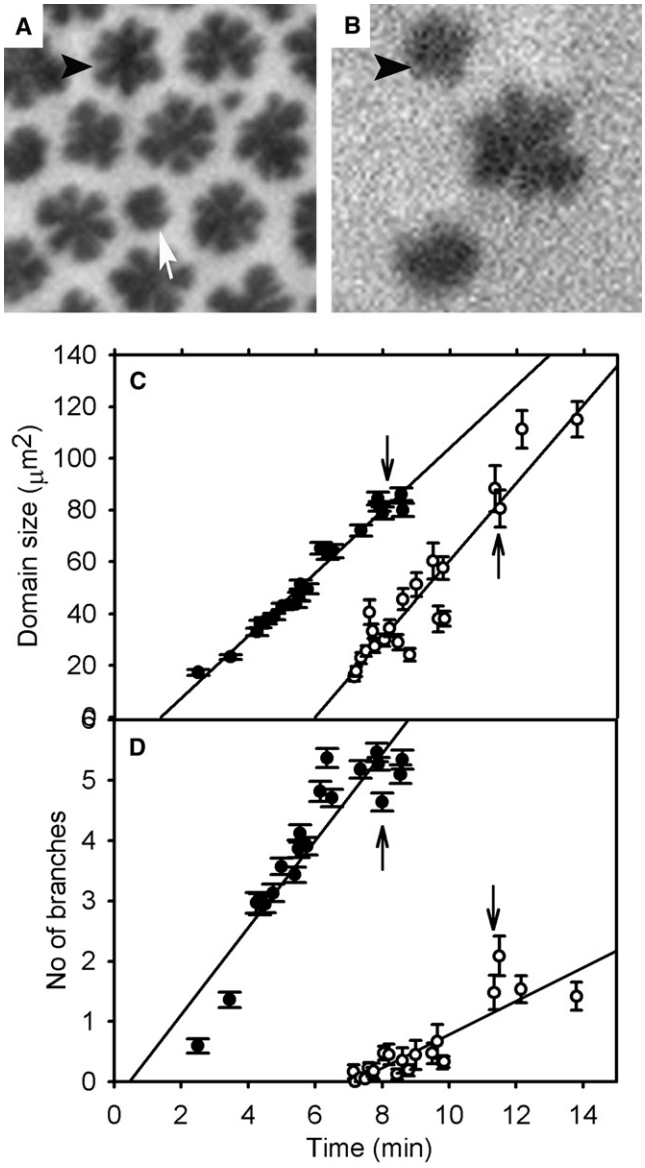

FIGURE 5 The complexity of Cer-enriched domain morphology does not directly depend on the domain growth rate. (*A–B*) Representative micrographies (50 × 50 μm) showing Cer-enriched domains of ~80μm^2 size (*black arrowheads*) formed under a fast (*A*) or slow (*B*) Cer production rate (3.2 ± 0.2 and 0.15 ± 0.05 × 10^{13} molec·cm^{-2}·min^{-1} respectively). The white arrow indicates a smaller domain that shows poor border undulation. (*C*) Domain growth curve for two experiments performed at fast (*solid circles*) or slow (*open circles*) Cer production rate. Domain growth rate is given by the slope of the linear regression curves yielding 12.1 ± 0.5 for the faster and 15 ± 1 μm^2·min^{-1} for the slower experiment. (*D*) Number of domain branches as shape parameter for the analysis of shape complexity for domains produced at fast (*solid circles*) or slow (*open circles*) Cer production rate experiment. The data is the average of 10–30 domains analyzed ± SE. Arrows indicate the punctual data where domains of comparable size (80μm^2) are analyzed.

the rotation symmetry parameter, *m* (32). Hartel and coworkers (16) reported the shape determinant dimensionless parameter $\Gamma = \mu^2/\lambda = 0.212 \pm 0.008$ and $A_c = 11 \pm 4\ \mu m^2$ for SMase-generated domains in the steady-state period of the SM→Cer catalytic conversion at a Cer production rate of 3.2 ± 0.2 × 10^{13} molec·min^{-1}·cm^{-2} (Table 1). The occurrence of successive shape transitions from circular to primary and secondary branched structures for Cer-enriched domains during SMase action was also reported (16). Hartel et al. calculated $A_c = 33\ \mu m^2$ and $\Gamma = 0.163 \pm 0.007$ for SM/Cer domains in an enzyme-free monolayer formed by spreading over the air/water interface a chloroform based solution of the pre-mixed lipids (Table 1). On the other hand, an earlier work (5) reports that enzyme-free SM/Cer monolayers of the same overall composition, showed more area occupied by the LC phase than when the domains were formed by the SMase-catalyzed reaction. This observation leads to the intuitive conclusion that Cer-enriched domains formed in an enzyme-free monolayer should contain a considerable proportion of SM molecules. Considering the data above and that experimental measurement of μ in pure SM or Cer monolayers yields that $\mu_{SM} < \mu_{Cer}$ (7.1 ± 0.4 and 13.2 ± 0.1 mD/Å^2 respectively), the larger value of $\Gamma = \mu^2/\lambda$ and the smaller value of A_c for the domains formed under SMase action can be attributed to a higher value of μ due to enrichment in Cer of the LC phase (Table 1). Further calculations, based on the average molecular area of SM and Cer molecules obtained from monolayer compression isotherm experiments, support that the domains formed in pre-mixed SM/Cer monolayers are composed of a near equimolar SM/Cer mixture (Cer mol fraction of 0.53 ± 0.06) whereas a similar analysis gives a value close to unity for the mol fraction of Cer in the SMase-acting domains at high Cer production rates (6). In further agreement with this data, Hartel et al. reported a highly structured hexagonal interdomain lattice formed under SMase activity that is not observed for SM/Cer domains formed in enzyme-free pre-mixed lipid monolayers (16). This effect can be explained as caused mainly by interdomain dipolar repulsion, induced by a higher content of the lipid component with a higher dipole moment (Cer) in SMase-generated domains (16).

The above data suggests that the shape annealing observed in the relaxation experiments shown in Figs. 2–4 can be attributed to a change of the overall resultant μ value of the LC domains as a consequence of a change in Cer content within the domains. To further test this hypothesis we studied the occurrence of a critical size in the domains formed in our relaxation experiments after shape annealing. Fig. 6 shows that the complexity of the domain shape after relaxation shows a dual behavior depending on the domain size. This indicates the presence of a critical size (after relaxation A_c) at ~95 μm^2 above which circular domains are no longer stable and border undulation occurs (see also Fig. 3, *right panel*). Fig. 6 also shows that the domain shape complexity (measured as P^2/A and number of branches) is always higher for domains of comparable size before relaxation than after relaxation, supporting a lower internal repulsion for the relaxed domains. From the data A_c ''after relaxation'' in

TABLE 1 Comparison of critical domain area and shape determinant parameters for SM/Cer monolayers at different equilibrium conditions

Sample	SMase activity, (molecules·cm^{-2}·min^{-1})	Critical domain area (Ac), (μm^2)	Shape transition exponent (Zm)‡	$\Gamma=\mu^2/\lambda$	Cer mole fraction§	μ_{LC}-μ_{LE} (mD/Å^2)¶
SMase acting on initially pure SM monolayers (fast)	3.2 ± 0.2 × 10^{13}	11 ± 4* 6 ± 2†	$Z_6 = 12.88/3$	0.212 ± 0.008* 0.23 ± 0.03†	LC phase ≈ 1 LE phase ≈ 0.02	6.1 ± 0.1
SMase acting on initially pure SM monolayers (slow)	0.15 ± 0.05 × 10^{13}	26 ± 7	$Z_4 = 11.76/3$	0.18 ± 0.01	—	—
SMase acting on initially SM/Cer (9:1) monolayers	3.0 ± 0.3 × 10^{13}	19 ± 5	$Z_4 = 11.76/3$	0.19 ± 0.01	—	—
After relaxation	0	95 ± 8	$Z_4 = 11.76/3$	0.162 ± 0.005	—	—
SM/Cer premixed monolayers	0	33 ± 13* 35 ± 19†	$Z_2 = 10/3$	0.163 ± 0.007* 0.160 ± 0.008†	LC phase 0.53 ± 0.06 LE phase ≈ 0.02	3.9 ± 0.1

*Taken from Hartel et al. (16).
†Value obtained by resampling Hartel's experimental data and treating it with the improved Active Contours Image Processing method used in this work.
‡Obtained from McConnell et al. (33).
§Obtained from De Tullio et al. (6)
¶Calculated from surface potential and average molecular area data from pure SM, pure Cer and SM/Cer (1:1) monolayer compression isotherms.

Fig. 6, we can calculate $R_c = (A_c/\pi)^{0.5}$=5.5μm. From the inset in Fig. 4 *A* we observed that a four symmetry domain shape is the more frequent shape for large domains (above A_c) after shape relaxation, thus a shape transition exponent Zm as $Z_4 = 11.76/3$ can be taken for our calculations (32).

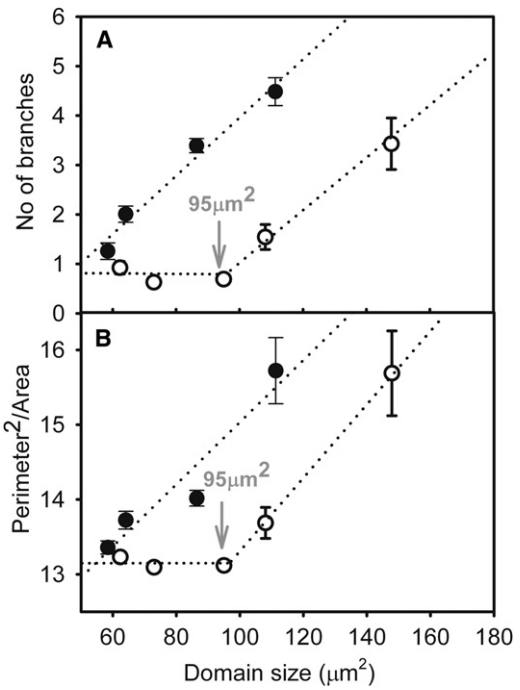

FIGURE 6 Assessment of the critical area for shape transition (circular to border undulated) for Cer-enriched domains after shape annealing. Shape parameters: number of branches (*A*), and perimeter^2/area (*B*) as a function of domain size before (*solid circles*) and after (*open circles*) relaxation. Dotted lines are drawn for eye guidance only and do not necessarily represent intermediate values between separate points. The values are an average of 20–60 domains ± SE.

The dipole distance between neighboring dipoles calculated by Hartel (16) as $d = 9.2$ Å^2 taking into account the average distance between the SM and Cer molecule is also valid for this case. Therefore, applying Eq. 2 we calculated Γ = 0.162 ± 0.005 for the SMase-generated domains after shape relaxation. This value is similar to that previously obtained for premixed SM/Cer monolayers and lower than the value reported for the SMase-generated domains during SMase action (Table 1).

The results shown in Table 1 suggest that the SMase-generated domains after shape annealing reach, due to incorporation of SM from the LE phase, a lipid composition closer to that of domains formed in the pre-mixed SM/Cer monolayer compared to that of SMase-generated domains under a rate of fast production of Cer. Careful phase separation studies in mixtures of Cer with POPC/SM/Chol indicated that Cer can recruit SM molecules into small gel-phase domains (12). Accordingly, and although no data or calculations were provided to support the statement, it was recently suggested that the increased domain area resulting from an increase in the proportion of Cer in enzyme-free DOPC/SM/Chol mixtures (as seen by atomic force microscopy) could be due to SM partitioning from the fluid phase into the segregated domains (20). If a compositional difference exists between the LC domains formed in premixed SM/Cer films and by SMase action as a consequence of a fast Cer production rate, then intermediate behavior should be expected in cases where Cer–enriched LC domains are formed at slow Cer production rate. To explore this hypothesis we studied the size dependence of the domain shape for several cases. Fig. 7 shows that the critical size for domain shape transition is larger for SMase-generated LC domains formed at a low Cer production rate (equivalent to the slower, near-to equilibrium experiment seen in Fig. 4) than that formed at high rate (Fig. 7, *A–B*) and smaller than that observed in

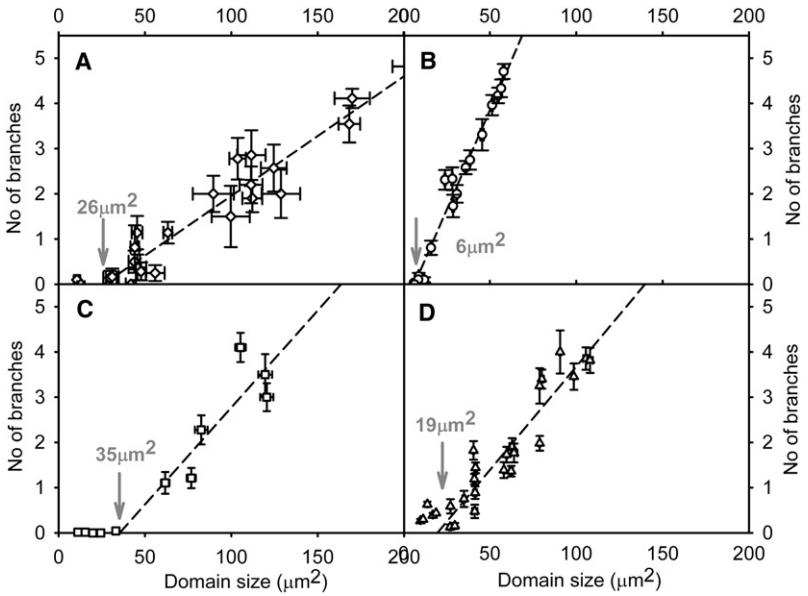

FIGURE 7 Assessment of the critical area for shape transition (circular to border undulated) for Cer-enriched domains at different equilibrium conditions. Domain shape is analyzed through the number of branches parameter (a value of 0 represent circularity) as a function of domain size. (*A*) Domains produced by slow SMase-driven SM→Cer conversion (two-dimensional enzymatic rate $0.15 \pm 0.05 \times 10^{13}$ molec·cm^{-2}·min^{-1}, equivalent to the slower experiment in Fig. 3) against initially pure SM monolayers; (*B*) Fast SM→Cer conversion by SMase ($3.2 \pm 0.2 \times 10^{13}$ molec·cm^{-2}·min^{-1}) against initially pure SM monolayers; (*C*) Average of domains present in premixed SM/Cer monolayers containing 2, 5 and 10 mol% of Cer (in the absence of SMase). (*D*) Fast SM→Cer conversion by SMase ($3.0 \pm 0.3 \times 10^{13}$ molec·cm^{-2}·min^{-1}) acting on premixed SM/Cer (9:1) monolayers. The data represents the average of 12–80 domains within a narrow size range ±SE.

SM/Cer premixed monolayers (Fig. 7 *C*). In addition, when SMase acts on premixed SM/Cer (9:1) monolayers that initially contain Cer-enriched domains, the value of A_c observed is also intermediate between the cases in Fig. 7, *B* and *C* even if the Cer production rate is high (Fig. 7 *D*). The latter result can be explained, within the framework proposed, as a consequence of the progressive addition of Cer molecules (as an out-of-equilibrium factor) to domains that were formed in near-equilibrium conditions (with a mol fraction of Cer ≈ 0.5). The analysis of those results are detailed in Table 1, where the experiments performed under intermediate equilibrium conditions (Fig. 7, *A* and *D*) yields values of Γ that are also intermediate.

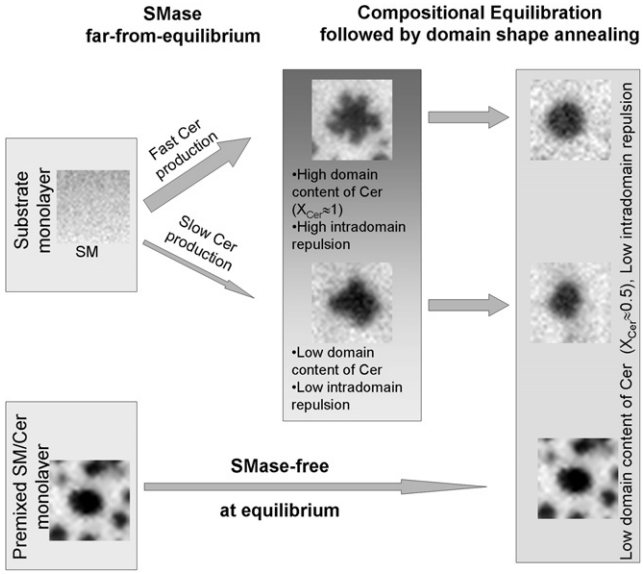

FIGURE 8 Schematic representation summarizing domain evolution both in a SMase-driven or enzyme free SM/Cer system.

CONCLUSIONS

In summary, the data supports an increased enrichment in Cer within the LC phase when domains are formed under fast production of Cer by SMase. The conclusions are summarized in Fig. 8. When SMase acts on a pure SM film (homogeneous LE phase) the Cer molecules produced accumulate in the LE phase, leading to supersaturation that acts as a driving force for domain nucleation (6). After the formation of stable nuclei of the new phase (LC) the subsequent Cer molecules being produced will partition into the previously formed LC domains in a way that depends on the rate of Cer production. A fast Cer production rate leads to an overshooted phase separation process in which the LC phase contains an initially higher proportion of Cer than that corresponding to the equilibrium composition of the LC phase. This behavior is similar to the supercooling effect of a rapidly cooled solution, resembling that reported for two-phospholipid system after a temperature quench to the LE-LC coexistence region (21,22). Within this context, the action of SMase can be taken as a surface perturbation that can induce a change in composition in the LE phase, driving the system to an out-of-equilibrium state depending on the rate at which Cer is being generated. As forces like intradomain dipolar repulsion and line tension acting at the domain boundary tend to compensate, different domain shapes are established that are sensitive to the dynamic LC phase composition. The consequence of this effect is the transient existence of highly undulated Cer-enriched domains dependent on the balance of the structural factors involved.

This work was supported in part by: Secretaria de Ciencia y Tecnologia (SECyT-UNC), Ministerio de Ciencia y Tecnología Córdoba (MinCyT-Cba), Consejo Nacional de Investigaciones Científicas y Técnicas (CONICET) and Fondo para la Investigación Científica y Tecnológica (FONCyT) some aspects of this investigation are inscribed within the PAE 22642

network in Nanobiosciences. B.M. and M.L.F. are Career Investigators of CONICET; L.D. is a Doctoral Fellow of CONICET. S.H. is supported by FONDECYT (1060890 & 7060265), and CONICYT (PBCT ACT47). J.J. is supported by FONDECYT (1060890 & 1030627). The Centro de Estudios Científicos (CECS) is funded by the Millennium Science Initiative and the Centers of Excellence Base Financing Program of CONICYT (Chile). CECS is also supported by a group of private companies which include Antofagasta Minerals, Arauco, Empresas CMPC, Indura, Naviera Ultragas and Telefónica del Sur.

REFERENCES

1. Edidin, M. 2003. The state of lipid rafts: from model membranes to cells. *Annu. Rev. Biophys. Biomol. Struct.* 32:257–283.
2. Huang, H. W., E. M. Goldberg, and R. Zidovetzki. 1996. Ceramide induces structural defects into phosphatidylcholine bilayers and activates phospholipase A2. *Biochem. Biophys. Res. Commun.* 220:834–838.
3. Burack, W. R., Q. Yuan, and R. L. Biltonen. 1993. Role of lateral phase separation in the modulation of phospholipase A2 activity. *Biochemistry.* 32:583–589.
4. Maggio, B., M. L. Fanani, C. M. Rosetti, and N. Wilke. 2006. Biophysics of sphingolipids ii. glycosphingolipids: an assortment of multiple structural information transducers at the membrane surface. *Biochim. Biophys. Acta.* 1758:1922–1944.
5. Fanani, M. L., S. Hartel, R. G. Oliveira, and B. Maggio. 2002. Bidirectional control of sphingomyelinase activity and surface topography in lipid monolayers. *Biophys. J.* 83:3416–3424.
6. De Tullio, L., B. Maggio, and M. L. Fanani. 2008. Sphingomyelinase acts by an area-activated mechanism on the liquid-expanded phase of sphingomyelin monolayers. *J. Lipid Res.* 49:2347–2355.
7. Goni, F. M., and A. Alonso. 2002. Sphingomyelinases: enzymology and membrane activity. *FEBS Lett.* 531:38–46.
8. van Blitterswijk, W. J., A. H. van der Luit, R. J. Veldman, M. Verheij, and J. Borst. 2003. Ceramide: second messenger or modulator of membrane structure and dynamics? Biochem. J. 369:199–211.
9. Clarke, C. J., and Y. A. Hannun. 2006. Neutral sphingomyelinases and NSMase2: bridging the gaps. *Biochim. Biophys. Acta.* 1758:1893–1901.
10. Holopainen, J. M., M. Subramanian, and P. K. Kinnunen. 1998. Sphingomyelinase Induces Lipid Microdomain Formation in a Fluid Phosphatidylcholine/Sphingomyelin Membrane. *Biochemistry.* 37:17562–17570.
11. Johnston, I., and L. J. Johnston. 2006. Ceramide promotes restructuring of model raft membranes. *Langmuir.* 22:11284–11289.
12. Silva, L. C., R. F. de Almeida, B. M. Castro, A. Fedorov, and M. Prieto. 2007. Ceramide-domain formation and collapse in lipid rafts: membrane reorganization by an apoptotic lipid. *Biophys. J.* 92:502–516.
13. Holopainen, J. M., H. L. Brockman, R. E. Brown, and P. K. Kinnunen. 2001. Interfacial interactions of ceramide with dimyristoylphosphatidylcholine: impact of the N-acyl chain. *Biophys. J.* 80:765–775.
14. Gulbins, E., and H. Grassme. 2002. Ceramide and cell death receptor clustering. *Biochim. Biophys. Acta.* 1585:139–145.
15. Cremesti, A. E., F. M. Goni, and R. Kolesnick. 2002. Role of sphingomyelinase and ceramide in modulating rafts: do biophysical properties determine biologic outcome? FEBS Lett. 531:47–53.
16. Hartel, S., M. L. Fanani, and B. Maggio. 2005. Shape transitions and lattice structuring of ceramide-enriched domains generated by sphingomyelinase in lipid monolayers. *Biophys. J.* 88:287–304.
17. De Tullio, L., B. Maggio, S. Hartel, J. Jara, and M. L. Fanani. 2007. The initial surface composition and topography modulate sphingomyelinase-driven sphingomyelin to ceramide conversion in lipid monolayers. *Cell Biochem. Biophys.* 47:169–177.
18. Fanani, M. L., and B. Maggio. 1998. Surface pressure-dependent cross-modulation of sphingomyelinase and phospholipase A2 in monolayers. *Lipids.* 33:1079–1087.
19. Montes, L. R., M. B. Ruiz-Arguello, F. M. Goni, and A. Alonso. 2002. Membrane restructuring via ceramide results in enhanced solute efflux. *J. Biol. Chem.* 277:11788–11794.
20. Johnston, I., and L. J. Johnston. 2008. Sphingomyelinase generation of ceramide promotes clustering of nanoscale domains in supported bilayer membranes. *Biochim. Biophys. Acta.* 1778:185–197.
21. Jorgensen, K., A. Klinger, and R. L. Biltonen. 2000. Nonequilibrium lipid domain growth in the gel-fluid two-phase region of a DC16PC-DC22PC lipid mixture investigated by Monte Carlo computer imulation, FT-IR, and fluorescence spectroscopy. *J. Phys. Chem. B.* 104:11763–11773.
22. de Almeida, R. F., L. M. Loura, A. Fedorov, and M. Prieto. 2002. Nonequilibrium phenomena in the phase separation of a two-component lipid bilayer. *Biophys. J.* 82:823–834.
23. Bianco, I. D., and B. Maggio. 1989. Interactions of neutral and anionic glycosphingolipids with dilauroylphosphatidylcholine and dilauroylphosphatidic acid in mixed monolayers. *Coll. Surf.* 40:249–260.
24. Fanani, M. L., and B. Maggio. 1997. Mutual modulation of sphingomyelinase and phospholipase A2 activities against mixed lipid monolayers by their lipid intermediates and glycosphingolipids. *Mol. Membr. Biol.* 14:25–29.
25. Fanani, M. L., and B. Maggio. 2000. Kinetic steps for the hydrolysis of sphingomyelin by *Bacillus cereus* sphingomyelinase in lipid monolayers. *J. Lipid Res.* 41:1832–1840.
26. Kass, M., A. Witkin, and D. Terzopoulos. 1988. Snakes: active contour models. *Int. J. Comput. Vis.* 1:321–331.
27. Xu, C., and J. L. Prince. 1998. Generalized gradient vector flow external forces for active contours signal processing. *Signal Process.* 71:131–139.
28. Miller, A., W. Knoll, and H. Mohwald. 1986. Fractal growth of crystalline phospholipid domains in monomolecular layers. *Phys. Rev. Lett.* 56:2633–2636.
29. Witten, T. A., and L. M. Sander. 1981. Diffusion-limited aggregation, a kinetic critical phenomenon. *Phys. Rev. Lett.* 47:1400–1403.
30. Sorensen, E. S., H. C. Fogedby, and O. G. Mouritsen. 1988. Crossover from nonequilibrium fractal growth to equilibrium compact growth. *Phys. Rev. Lett.* 61:2770–2773.
31. Vanderlick, T. K., and H. Mohwald. 1990. Mode selection and shape transition of phospholipid monolayer domains. *J. Phys. Chem.* 94:886–890.
32. McConnell, H. M. 1990. Harmonic shape transitions in lipid monolayer domains. *J. Phys. Chem.* 94:4728–4731.
33. McConnell, H. M. 1991. Structures and transitions in lipid monolayers at the air-water interface. *Annu. Rev. Phys. Chem.* 42:171–195.